Acta Cryst. (1976). A32, 551

Intergrowth Tungsten Bronzes

BY ALTAF HUSSAIN AND LARS KIHLBORG

Department of Inorganic Chemistry,
Arrhenius Laboratory, University of Stockholm, S-104 05 Stockholm, Sweden

(*Received* 3 *November* 1975; *accepted* 13 *January* 1976)

A series of phases has been found in the tungsten bronze systems M_xWO_3 for $x \leq 0{\cdot}10$ when M = K, Rb, Cs, Tl. The crystal structure of one of these was derived from a high-resolution electron micrograph (lattice image) and confirmed by X-ray diffraction analysis. It can be considered as an (ordered) intergrowth of slices of hexagonal tungsten bronze type with slabs of WO_3 structure type. Different members of the series characterized by different thicknesses of the WO_3 slabs have been observed. Members have been obtained only intermixed with others, never as single phases. Disorder in the form of varying widths of the two structure elements has been observed quite frequently.

1. Introduction

The tungsten bronzes form a group of largely non-stoichiometric compounds of general formula M_xWO_3, where M is an electropositive element, typically an alkali metal. Three structure types have been reported, *viz.* defect perovskite (cubic or distorted) (Hägg, 1935; Magnéli, 1951), tetragonal potassium tungsten bronze type (TTB) (Magnéli, 1949) and hexagonal tungsten bronze type (HTB) (Magnéli, 1953), shown in Fig. 1. The perovskite-type bronzes are formed with the smallest alkali metals Li and Na, the TTB-type with Na and K while the HTB-type can be obtained with K, Rb and Cs. Many elements besides the alkali metals for example Tl (Sienko, 1959; Bierstedt, Bither & Darnell, 1966) have been found to form tungsten bronzes. A recent review by Hagenmuller (1973) may be consulted for more information.

While the perovskite-type bronzes have been rather extensively studied, the two other types have not. Most of the composition ranges for the TTB and HTB phases originally reported by Magnéli & Blomberg (1951) have since been extended by others; the latest published values are given in Table 1.

There seems to have been no systematic study of the phase relationships in these systems, however, and this led us to undertake an investigation of the ranges of composition as a function of temperature for the K, Rb and Cs phases. We have found approximately the same lower limit of composition, $x \simeq 0{\cdot}13$, for the HTB phase in all these systems. A full account of the phase analysis will be published elsewhere. We report here on a family of new phases which we have observed for low x values in the course of these studies.

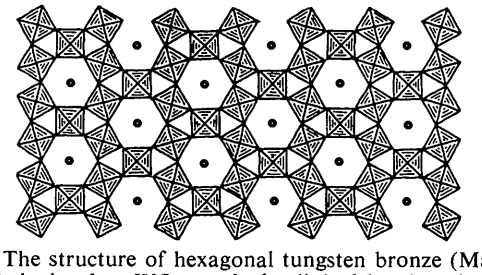

Fig. 1. The structure of hexagonal tungsten bronze (Magnéli, 1953) depicted as WO_6 octahedra linked by shared corners with alkali metal atoms in the hexagonal tunnels formed.

Table 1. *Reported compositial regions of formation for tetragonal and hexagonal tungsten bronzes,* M_xWO_3

M	Structure	x	Reference
Na	TTB	0·26–0·35	Réau *et al.* (1970)
K	TTB	0·40–0·59	Réau *et al.* (1970)
	HTB	0·13–0·31	Banks & Goldstein (1968)
Rb	HTB	0·20–0·33	Wanlass & Sienko (1975)
Cs	HTB	~0·30–0·32	Magnéli (1953)
Tl	HTB	~0·30	Bierstedt *et al.* (1966)
In	HTB	0·2—0·3	Bouchard & Gillson (1968)

2. Preparation

Samples of composition M_xWO_3 were prepared from mixtures of appropriate amounts of tungsten trioxide (prepared by dehydration of tungstic acid, Merck, puriss), tungsten dioxide (prepared from WO_3 by reduction with a H_2/H_2O mixture) and alkali or thallium tungstate. Potassium tungstate was commercially available (BDH, reagent grade) but rubidium, caesium and thallium tungstate had to be prepared from tungsten trioxide and the corresponding carbonate (reagent grade) by heating in a platinum crucible for 5–6 h at 950 °C. The mixtures were heated in sealed, evacuated silica tubes, sometimes with an inner platinum capsule, at 700–950 °C for various periods of time.

3. Results

Microscopic examination revealed the presence of relatively large, black crystals or crystal aggregates in the samples of gross compositions $0{\cdot}01 \leq x \leq 0{\cdot}12$ which had been heated at 800–950 °C for 4 h or longer. At low x values there were only a few crystals

in a mass of yellow-white, very fine powder, which was mainly WO_3 to judge from its X-ray powder pattern. The proportion of the black crystals increased with x; samples with $x=0{\cdot}10$ contained only minute amounts of the light, fine powder. In the region $0{\cdot}10<x<0{\cdot}13$ these crystals occurred together with a phase which, from its appearance under the microscope and from its powder pattern, was found to be hexagonal tungsten bronze, HTB. At $x=0{\cdot}13$ the HTB phase was single.

The black crystals were not affected by treatment with hot, strong alkaline solutions or by acids, and these agents could therefore be used to separate this phase from the fine grained powder (WO_3) which was readily dissolved in alkali. In this respect the crystals resembled the tungsten bronzes and they will hereafter be called *intergrowth tungsten bronzes*, ITB, for reasons that will become obvious later in this article.

The intergrowth bronzes formed elongated, flaky crystals with shining faces. They normally appeared black and opaque but examination at high magnification in a light microscope revealed that they were translucent with a greenish colour in thin sections. The ITB phases with different alkali metals, or thallium, behaved similarily in this respect.

The alkali/tungsten ratio was determined in crystals of the potassium phase. For this purpose a scanning electron microscope equipped with an EDAX energy-dispersive analysis attachment was used. A sample of hexagonal potassium tungsten bronze was used as a standard. Its composition according to the synthesis (formed as a single phase in a closed system) was $K_{0{\cdot}15}WO_3$ and an analysis using the standard X-ray fluorescence analysis technique gave $x=0{\cdot}14$.

The ITB crystals were taken from a sample prepared from the composition $K_{0{\cdot}10}WO_3$ which contained practically no WO_3. The EDAX analysis gave the value $x=0{\cdot}10\pm0{\cdot}01$.

A comparison was also made of the alkali content in crystals from a Rb_xWO_3 sample before and after purification in alkali and acids. That no significant difference was found indicates that no alkali is leached out by this treatment.

The X-ray powder patterns of the ITB samples were very complex; a typical pattern is listed in Table 2. The indexing will be discussed later in this article.

4. Electron microscopic studies

The electron optical investigations were made with a Siemens ELMISKOP 102 equipped with a double tilt–lift stage using 125 kV acceleration potential. The specimens were prepared by gentle crushing of the crystals in an agate mortar and collection of the resulting powder, dispersed in n-butanol, on holey carbon films supported by standard copper grids. Electron diffraction patterns were used for alignment of the crystal precisely along a crystallographic axis. Lattice images were recorded of thin parts projecting over a hole in the support film, by the technique, which Iijima (1971) *inter alia* has described.

The electron diffraction patterns indicated orthorhombic lattices with one long axis a of the order of 20–30 Å and two shorter, $b=7{\cdot}4$ and $c=7{\cdot}6$ Å, the latter with a marked subaxis $c'=3{\cdot}8$ Å. Patterns with different a axes were observed (see below) but one with $a\simeq27{\cdot}6$ Å seemed most frequent.

With the crystal oriented with the c axis parallel to the beam, lattice images such as that shown in Fig. 2 were observed for the phase with $a\simeq27{\cdot}6$ Å. It has been shown (Cowley & Iijima, 1972; O'Keefe, 1973) that two-dimensional lattice images of thin crystals represent, under proper imaging conditions, the projected potential or, roughly, the projected charge density of the crystal. In the present case the image in Fig. 2 could be interpreted naively in terms of the structure model shown in Fig. 3. This interpretation was subsequently verified by the single-crystal X-ray study described below, and also by the agreement between the observed and calculated images (Fig. 4). These latter were computed from the model by use of the multislice method (Cowley & Moodie, 1957; Goodman & Moodie, 1974) with the aid of a computer program originally written by P. Fejes and J. Skarnulis at Arizona State University, Tempe, Arizona, U.S.A. Further results of image calculations, extended to include also other ITB phases and other alkali atoms, will be presented in a separate article.

5. The structure model

The idealized structure model derived from the electron microscopic image is shown in Fig. 3. The structure can be regarded as an ordered intergrowth of slabs of HTB type (Fig. 1) with slabs of ReO_3-(WO_3) type. The width of the HTB slices is such as to include two rows of hexagonal tunnels, while the WO_3 slabs are three octahedra thick. The octahedra in the WO_3 slabs have been tilted by an angle 15° in alternating sense to make the two elements fit together perfectly. This tilting makes the WO_3 structure more compact,

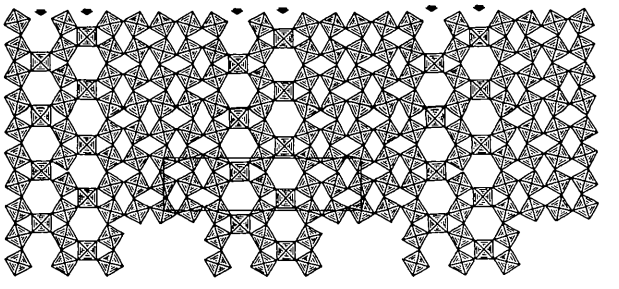

Fig. 3. Structure model derived from the image in Fig. 2. WO_6 octahedra linked by corner sharing. The alkali metal atoms in the hexagonal tunnels not indicated. The HTB elements have been extended downwards for sake of clarity, the planes of 'inserted octahedra' (see text) are indicated by arrows.

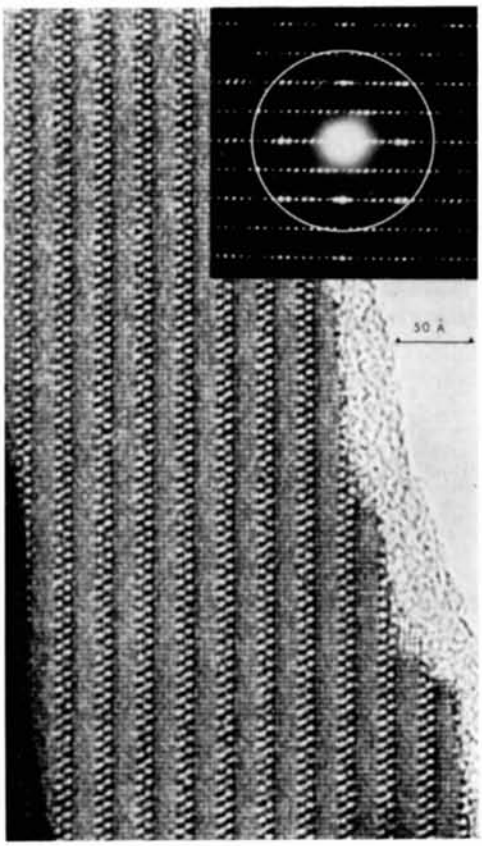

Fig. 2. Lattice image of a thin edge of a crystal of the (1,5) ITB phase from a sample of composition $K_{0\cdot10}WO_3$. Corresponding diffraction pattern also shown, with the size of the objective aperture indicated.

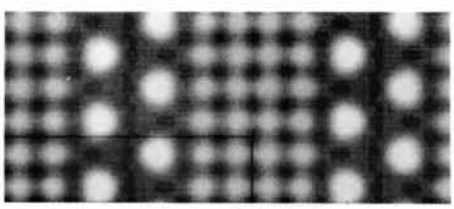

Fig. 4. Synthetic image calculated from the structure model of Fig. 3 by 'multislice' computation for 280 beams through 9 slices of the crystal (thickness $9\times3\cdot88=34\cdot9$ Å). Incident-beam convergence (max. $2\cdot0\times10^{-3}$ rad) taken into account by calculation for 13 beam directions over a quarter of the condenser aperture and summation of the image intensities after symmetry expansion (O'Keefe & Sanders, 1975). Defocus -750 Å; spherical aberration constant $C_s=2\cdot20$ mm; focus spread (due to chromatic aberration) $=100$ Å; the objective aperture size corresponds to a radius of $0\cdot42$ Å^{-1} in reciprocal space (105–112 beams through the aperture).

[*To face p.* 552

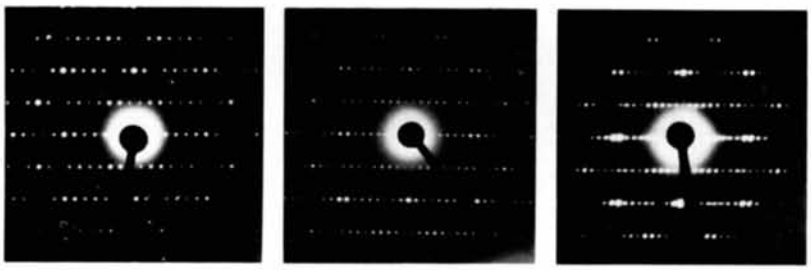

Fig. 7. Electron diffraction patterns (*hk*0 zones) from ITB crystals of type (1,4), (1,6) and (1,7).

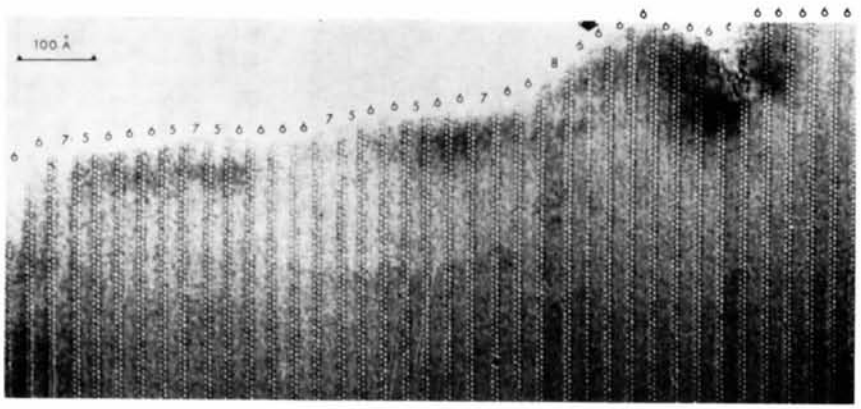

(*a*)

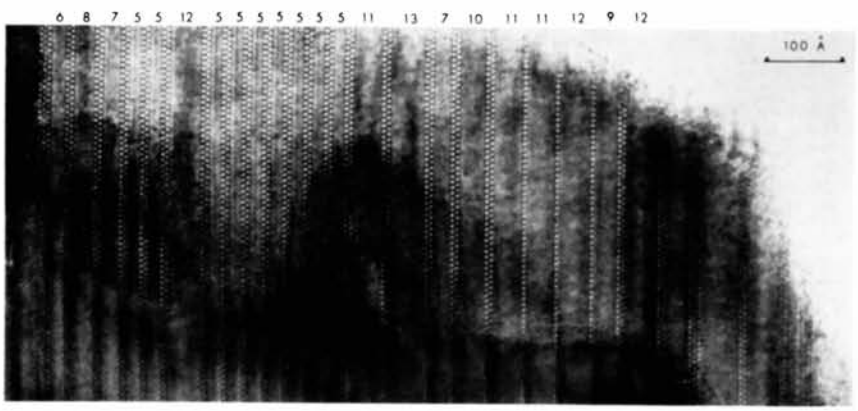

(*b*)

Fig. 8. Lattice images from Rb_xWO_3 crystals in a sample with $x=0{\cdot}03$. The widths of the WO_3 slabs in terms of n are given above each slab. (*a*) A moderately disordered crystal where the tunnel rows are double with only one exception (indicated by an arrow. (*b*) A highly disordered fragment with both single, double and triple tunnel rows and large variation of the distance between these.

Table 2. *Powder pattern from a sample* $K_{0.10}WO_3$ *prepared at* 800 °C (15 h)

Obtained with a Guinier–Hägg focusing camera and Cu $K\alpha_1$ radiation ($\lambda = 1{\cdot}54051$ Å). KCl was added as internal standard ($a = 6{\cdot}2919$ Å). The indexing and calculated $\sin^2\theta$ values are based on the lattice parameters of the three ITB phases given in Table 4.

		$(1,4)_2$ Phase		$(1,5)_1$ Phase		$(1,6)_2$ Phase	
Intensity (obs)*	$\sin^2\theta \times 10^5$ (obs)	*hkl*	$\sin^2\theta \times 10^5$ (cal)	*hkl*	$\sin^2\theta \times 10^5$ (cal)	*hkl*	$\sin^2\theta \times 10^5$ (cal)
vvw	719			300	714		
vvw	984					001 800	985 985
vvw	1048					201	1047
vvw	1114					110	1113
m	1182			110	1182		
m	1237					310	1237
vw	1272			400	1269		
vvw	1349	310	1351				
s	1418			210	1420		
m	1485					510	1483
w	1531					10,0,0	1540
m	1817			310	1816		
w	1850					710	1852
w	1986			500	1982	801	1971
w	2215					12,0,0	2217
vvw	2354	311	2343	410	2371	910	2345
vvw	2649	10,0,0	2648				
w	2858			600	2854		
vw	2953			501	2968		
vw	3016					14,0,0	3018
vw	3082			510	3085		
w	3698					13,1,0	3700
vsb	3867	12,0,0	3813	700	3885		
						16,0,0	3941
	3944	002	3967	002	3943	002	3941
vvw	4007					14,0,1	4003
vs	4406	020	4450	020	4410	020	4392
s	4491			120	4490	602	4495
vw	4561	220	4557			15,1,0	4562
vw	4645			302	4656	420	4659
vvw	4730			220	4728		
s	4979					18,0,0	4988
s	5066			800	5074	112	5054
m	5125			112 320	5124 5124		
m	5194	14,0,0	5190			312	5178
wb	5359			212	5362	820	5378
vvw	5427					512	5424
vw	5472	221	5449	121	5476	10,0,2	5481
s	5667	802	5662	420	5679		
m	5748	512	5742	312	5759		
m	5800					712	5793
m	5929			502	5925		
m	6143	820	6146			12,0,2	6158
m	6280					912	6286
s	6405			520	6393		
s	6609	10,0,2	6615			12,2,0	6609
vw	6786	16,0,0	6786	602	6798		
vvw	6903					11,1,2	6902
m	7267			620	7265		
w	7431			901	7407	14,2,0	7410
w	7634					13,1,2 19,1,1	7641 7641
m	7815			702	7827		
m	7869					16,0,2	7882
vsb	8291	12,2,0	826	720	8295		
	8366			022	8353	16,2,0	8334
						022	8332
m	8416	022	8418	122	8432		
s	8922			712 10,0,1	8930 8914	203 18,0,2	8929 8929
s	9007			802	9017		
vvw	9316					822 16,2,1	9349 9349

Table 2 (*cont.*)

Intensity (obs)*	$\sin^2\theta\times10^5$ (obs)	$(1,4)_2$ Phase *hkl*	$\sin^2\theta\times10^5$ (cal)	$(1,5)_1$ Phase *hkl*	$\sin^2\theta\times10^5$ (cal)	$(1,6)_2$ Phase *hkl*	$\sin^2\theta\times10^5$ (cal)
m	9383					18,2,0	9380
s	9479			820	9484	17,1,2	9488
m	9614	14,2,0	9641	422	9622		
m	9881	603	9880			10,2,2	9873
vvw	10003			130	10003		
vw	10085	113	10067			20,0,2 313	10099 10104
m	10339			522	10335		

* *v*=very, *w*=weak, *m*=medium, *s*=strong, *b*=broad.

as the O atoms in the equatorial plane increase their anion coordination from 8 to 9 and the volume is reduced by 6·7%, ideally. The O positions in this plane conform to one of Wells's five-connected nets (Wells, 1962).

Alternatively, the structure can be looked upon as a WO_3 structure with tilted octahedra into which additional octahedra have been inserted along parallel planes (indicated by arrows in Fig. 3), to create large holes (tunnels) for the alkali metal atoms.

The symmetry of this model is orthorhombic, of two-dimensional space group *pgm*. If the atoms are assumed to be located on mirror planes at $z'=0$ and $z'=\frac{1}{2}$ referring to the short c' subaxis, the full symmetry is then *Pbm*2 (No. 28 in *International Tables for X-ray Crystallography*, 1952).

The ideal unit-cell dimensions, based upon the known a parameter for the HTB structure ($a=$ 7·387 Å) and upon the assumption of regular octahedra, are $a=27{\cdot}57$, $b=7{\cdot}387$, $c'=3{\cdot}824$ Å. Except for the weakly expressed doubling of the c axis, the approximate parameters obtained from the electron diffraction patterns were in agreement with these values. The c axis is also doubled in the HTB structure (Magnéli, 1953).

6. X-ray diffraction studies

In order to verify this model by a conventional structure analysis, crystals were examined by the X-ray diffraction technique. Most of the crystals selected were composite, however, *i.e.* gave patterns formed by two or more lattices with the same b and c parameters but different length of the a axis.

One reasonably good single crystal was eventually found in a sample of gross composition $K_{0.10}WO_3$ and from it a preliminary X-ray analysis was made. The Weissenberg patterns confirmed the orthorhombic symmetry. The doubling of the c axis was indicated by extremely faint spots.

Intensities of $hk0$ reflexions for $\theta<42°$ within one quadrant were measured with a single-crystal diffractometer (Siemens AED with graphite monochromator), Cu $K\alpha$ radiation, and θ–2θ scan (five-values measurement). The size of the crystal was 2·2 (along a), 54·2 (b), 18·7 μm (c) and absorption corrections were applied (linear absorption coefficient $\mu=963{\cdot}8$ cm^{-1}). This shape is typical for the ITB crystals. Least-squares refinement in projection was performed with orthorhombic symmetry assumed and the ideal atomic positions of the model used as starting parameters. This refinement gave a conventional R value of 0·12 and the resulting atomic positions did not deviate much from those of the model, as is evident from Table 3. The result of a difference Fourier synthesis in which the calculated contribution from the W atoms had been subtracted is presented in Fig. 5. Peaks corresponding to the O atoms appear clearly, they demonstrate the tilt of the octahedra.

Table 3. *Positional parameters obtained from the two-dimensional refinement for* $K_{0\cdot1}WO_3$ – *ITB* (1,5)

Standard deviations in the last digits within parentheses. Equivalent positions: x,y; $\bar{x},\bar{y}$; $\bar{x},\frac{1}{2}+y$; $x,\frac{1}{2}-y$.

All these atoms have $z'\simeq0$. In addition, there are four O atoms at $z'\simeq\frac{1}{2}$ with approximately the same x and y coordinates as the W atoms.

	x	*y*
W(1)	0·0	0·0
W(2)	0·135 (1)	0·0
W(3)	0·384 (1)	0·75
W(4)	0·270 (1)	0·0
O(1)	0·066 (4)	0·967 (13)
O(2)	0·200 (4)	0·026 (12)
O(3)	0·340 (4)	0·922 (12)
O(4)	0·437 (4)	0·906 (13)
O(5)	0·011 (5)	0·25
O(6)	0·123 (5)	0·25
O(7)	0·286 (5)	0·25
O(8)	0·474 (5)	0·25
O(9)	0·141 (5)	0·75
O(10)	0·266 (5)	0·75
K(1)	0·382 (12)	0·25

Only some very small maxima appear on this map within the hexagonal tunnels where the K atoms should be. There is, however, a broad positive area around these peaks of density less than the lowest contour level. This feature might indicate that the K atoms are located within the tunnels but are off-centre, possibly disordered.

An attempt to refine the occupancy g and temperature factor B for the K atom in position $(0{\cdot}38,\frac{1}{4})$ yielded $g=0{\cdot}12\pm0{\cdot}10$ (full occupancy: $g=\frac{1}{2}$) and $B=4\pm12$ Å^2. The large standard deviations suggest that these parameters are not determinable; this too may indicate that the alkali atoms do not occupy the assumed centre position.

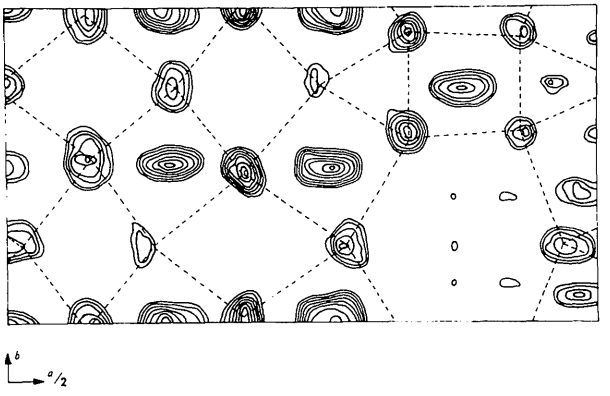

Fig. 5. Difference Fourier map (projection along c) with contribution from the tungsten atoms subtracted. Oxygen positions (from Table 3) connected to show the extension of the octahedra.

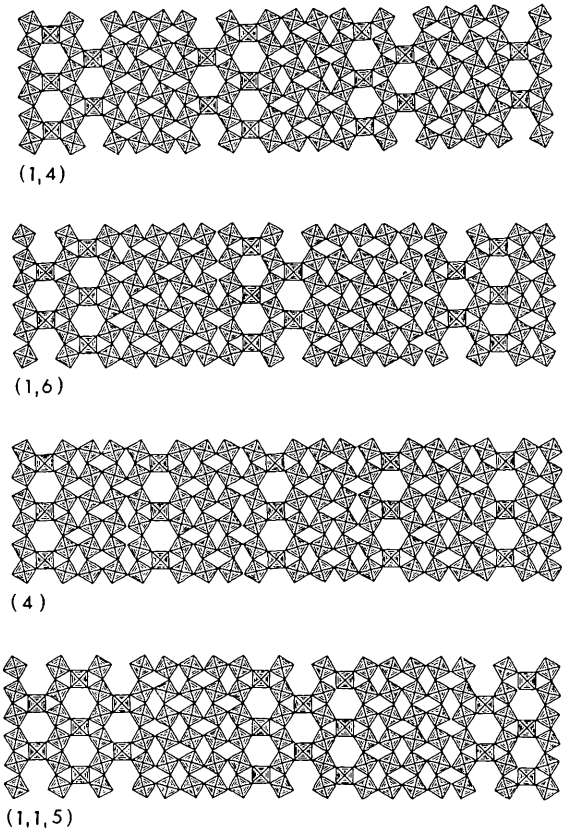

Fig. 6. The (idealized) structures of some ITB phases. The two lower ones are hypothetical.

7. Family of homologous structures

It was already clear from the first electron diffraction patterns that several closely related structures exist, one of which is that derived above. This is readily understandable from the structure model. Here, as for other intergrowth structures, a whole family of phases which differ only in the widths of the two types of structure elements can be proposed. If the description in terms of planes of extra octahedra inserted in a WO_3 structure (see above) is used, the members of this family can be identified most generally by a group of numbers, $m,n,p,\ldots$, which designate the number of rows of octahedra *between* the inserted planes, surrounded by parentheses to indicate a repeating sequence.

Because of the tilt of the octahedra, the tunnels in two adjacent rows will be at the same y level if there is an even number of octahedral rows between, but will be displaced by $\Delta y=\frac{1}{2}$ relative to each other if an odd number of rows intervenes. This should be evident from Fig. 6. It implies that for $m+n+p+\ldots=$even, the parentheses enclose a full repeat sequence in an orthogonal cell; this can be designated by a subscript $r=1$, *e.g.* $(m,n,p,\ldots)_1$. For $m+n+p+\ldots=$odd, $r=2$, indicating that the sequence within the parentheses has to be taken twice to correspond to the repeat a perpendicular to the planes, so that the cell is C-centred orthogonal.

The structure described above is accordingly designated as $(1,5)_1$ and the HTB structure itself as $(1)_2=(1,1)_1$. In the reasonably well-ordered regions of the crystals observed so far, only type $(1,n)$ has been seen, *i.e.* structures with double rows of tunnels like that in Fig. 2. Of 15 crystal fragments of potassium ITB phase from a sample with $x=0{\cdot}10$ studied in the electron microscope, there were 6-type (1,4), 8-type (1,5) and 1-type (1,6). These members also occur in the Rb and Cs systems. Typical diffraction patterns are shown in Fig. 7. The predominant n value and the average composition x seem correlated, such that the higher n values are more frequent at low x values. This is reasonable since $x_{max}=1/(2+n)$ for $(1,n)$ structures with alkali atoms occupying the tunnel sites. All samples obtained so far have been mixtures of crystals with different n values, however, which is a reason why the powder patterns are very complex.

The general expression for the length of the a axis for a member of the family $(m,n)_r$ in terms of the a axis for the HTB bronze, a_{HTB}, is $a=a_{HTB}[(m+n)/2+1/\sqrt{1+\sqrt{\frac{3}{2}}}]r\approx3{\cdot}694(m+n+1{\cdot}464)r$ Å ($r=1$ when $m+n=$even, $r=2$ for $m+n=$odd). Some values calculated with this expression are given in Table 4. The powder pattern listed in Table 2 can be indexed if it is assumed that the sample is a mixture of (1,4), (1,5) and (1,6). The resulting cell dimensions are given in Table 4.

Investigation of the conditions governing formation of the various members is under way.

8. Disorder

As expected for a structure of this kind, various sorts of disorder are observed, from isolated faults where a slab of 'wrong' width has grown in an otherwise regular structure to cases in which slabs of different widths alternate in a quite irregular sequence. It is mainly the width of the WO_3 elements that varies. The HTB elements two rows of tunnels in thickness are by far the most frequent and seem to possess a particular stability, but single and triple rows of tunnels have also been observed. Fig. 8(*a*) shows an example of a disordered fragment where mainly the WO_3 elements vary. In Fig. 8(*b*) the variation is much larger and includes both the WO_3 and the HTB slabs.

It was mentioned above that most of the crystals selected for X-ray investigation gave composite patterns. This shows that relatively large, well ordered regions of different members grow together coherently.

Disorder seems to be most common in the Rb system and in samples heat treated for short times. A further discussion of disorder in the ITB structures must, however, await the results of studies now under way.

9. Discussion

Réau *et al.* (1970) have reported an orthorhombic phase in the K system K_xWO_3 with $0{\cdot}06 < x < 0{\cdot}09$, forming at about 750°C. From the general appearance of the X-ray diffraction patterns they propose a structure formed simply by inserting K atoms in the voids of a WO_3 framework along parallel planes. The reported unit-cell dimensions (Table 4) and powder diffraction intensities make it seem plausible that this is the member $(1,8)_2$ of the ITB family. The expected (ideal) repeat distance for this member is $a = 2 \times 38{\cdot}65$ Å. The doubling was not observed by Réau *et al.* However, for a phase with n as high as 8 the reflexions with h odd are expected to be weak and could easily have escaped observation. It is also possible that in a structure with WO_3 slabs as wide as these the tilt of the octahedra gradually decreases towards the middle of the slabs and reverses there. The (100) mirror plane in the middle of the slabs (*cf.* the two upper models of Fig. 6) would then be replaced by glide planes which would remove the doubling of a and change the symmetry from *cm* to *pg*. Such 'inversions' have in fact been observed by us as local faults in $Rb_{0{\cdot}03}WO_3$ crystals. If such faults were frequent the odd reflexions would be diffuse and easily overlooked.

Steadman, Tilley & McColm (1972) have prepared a number of phases in the Sn–WO_3 system, tin tungsten bronzes with compositions Sn_xWO_3 $0{\cdot}01 \le x \le 0{\cdot}3$. They designate these phases '5-type', '6-type', *etc.* where the number refers to the characteristic periodic intensity variation in the diffraction photographs. From preliminary X-ray diffraction and electron microscopy studies they propose structure models for these phases. These are only substructures, however, since all phases have large, unknown superstructures whose size differ among the various phases.

The structure models suggested for the '5-type' and '6-type' are identical with the (1,2) and (1,3) ITB structures, respectively. The compositions are given as $Sn_{0{\cdot}3}WO_3$ for the '5-type' and $Sn_{0{\cdot}2}WO_3$ for the '6-type', although no precise analysis has been reported. According to this the tin content in these compounds is thus considerably higher than the alkali content in the ITB phases; for the '5-type' even higher than can be accommodated in the tunnels. In fact, Steadman *et al.* (1972) find no experimental evidence for the Sn atoms occupying tunnel sites and suggest that they are more or less randomly distributed over the octahedral sites. This would require a much higher oxygen-to-metal ratio, however, so that the situation is still unclear.

The structures they suggest for the 'N-types' with $N \ge 7$ differ substantially from the lower-type structures. However, the metal atom arrangments in the suggested structures are very close to those of the

Table 4. *Comparison of observed and calculated unit-cell dimensions* (Å) *for several ITB (or may-be ITB) phases*

Calculated values are based on the lattice parameters of the potassium HTB bronze. $b_{cal} = 7{\cdot}387$, $c_{cal} = (2\times)\ 3{\cdot}755$ Å for all the phases.

	a_{cal}	a_{obs}	b_{obs}	c_{obs}	Note
$(1,2)_2$	$2\times 16{\cdot}49$	$2\times 16{\cdot}62$	7·125	$14\times 3{\cdot}795$	1
(1,3)	20·18	20·40	7·415	$12\times ?{\cdot}787$	1
$(1,4)_2$	$2\times 23{\cdot}88$	$2\times 23{\cdot}67$ (4)	7·30 (1)	$2\times 3{\cdot}867$ (5)	2
(1,5)	27·57	27·356 (9)	7·335 (2)	$2\times 3{\cdot}879$ (2)	2
$(1,6)_2$	$2\times 31{\cdot}27$	$2\times 31{\cdot}04$ (1)	7·351 (3)	$2\times 3{\cdot}880$ (1)	2
$(1,8)_2$	$2\times 38{\cdot}65$	38·50	7·35 (1)	3·88 (1)	3
(6)	24·86	$(2\times)25{\cdot}05$	7·372	$10\times 3{\cdot}896$	4
$(7)_2$	$2\times 28{\cdot}56$	$(2\times)28{\cdot}92$	7·373	$10\times 3{\cdot}89$	4

(1) 5- and 6-type tin–tungsten bronzes of Steadman, Tilley & McColm (1972).
(2) Potassium ITB phases. This investigation.
(3) K_xWO_3 phase of Réau *et al.* (1970).
(4) 7- and 8-type tin–tungsten bronzes of Steadman, Tilley & McColm (1972), only tentatively assigned to the ITB family here.

(n) ITB structures with $n=N-1$, *i.e.* structures where the rows of hexagonal tunnels are *single* instead of double. The reported unit-cell dimensions are in agreement with those calculated for such ITB structures (see Table 4).

The huge superstructures as well as the presence of diffuse reflexions, indicating disorder, seem to have limited the structural information available so far for the tin tungsten bronzes.

We have started a thorough X-ray analysis of a caesium ITB crystal. Studies of the physical and chemical properties of the ITB phases are also underway.

This investigation is a part of a research program supported by the Swedish Natural Research Council. A. H. acknowledges fellowships from the International Seminar in Chemistry at Uppsala University and from the Swedish Institute.

References

BANKS, E. & GOLDSTEIN, A. (1968). *Inorg. Chem.* **7**, 966–969.
BIERSTEDT, P. E., BITHER, T. A. & DARNELL, F. J. (1966). *Solid State Commun.* **4**, 25–26.
BOUCHARD, R. J. & GILLSON, J. L. (1968). *Inorg. Chem.* **7**, 969–972.
COWLEY, J. M. & IIJIMA, S. (1972). *Z. Naturforsch.* **27a**, 445–451.
COWLEY, J. M. & MOODIE, A. F. (1957). *Acta Cryst.* **10**, 609–619.
GOODMAN, P. & MOODIE, A. F. (1974). *Acta Cryst.* A**30**, 280–290.
HAGENMULLER, P. (1973). *Comprehensive Inorganic Chemistry*. Vol. 4. Edited by J. C. BAILAR, H. J. EMELEUS, R. NYHOLM & A. F. TROTMAN-DICKENSON. Oxford: Pergamon Press.
HÄGG, G. (1935). *Z. phys. Chem.* (*B*), **29**, 192–204.
IIJIMA, S. (1971). *J. Appl. Phys.* **42**, 5891–5893.
International Tables for X-ray Crystallography (1952). Vol. I. Birmingham: Kynoch Press.
MAGNÉLI, A. (1949). *Ark. Kem.* **1**, 213–221.
MAGNÉLI, A. (1951). *Acta Chem. Scand.* **5**, 670–672.
MAGNÉLI, A. (1953). *Acta Chem. Scand.* **7**, 315–324.
MAGNÉLI, A. & BLOMBERG, B. (1951). *Acta Chem. Scand.* **5**, 372–378.
O'KEEFE, M. A. (1973). *Acta Cryst.* A**29** 389–401.
O'KEEFE, M. A. & SANDERS, J. V. (1975). *Acta Cryst.* A**31**, 307–310.
RÉAU, J. -M., FOUASSIER, C., LE FLEM, G., BARRAUD, J. -Y., DOUMERC, J. -P. & HAGENMULLER, P. (1970). *Rev. Chim. Minér.* **7**, 975–988.
SIENKO, M. J. (1959). *J. Amer. Chem. Soc.* **81**, 5556–5559.
STEADMAN, R. (1972). *J. Chem. Soc. Dalton*, pp. 1271–1273.
STEADMAN, R., TILLEY, R. J. D. & MCCOLM, I. J. (1972). *J. Solid State Chem.* **4**, 199–208.
WANLASS, D. R. & SIENKO, M. J. (1975). *J. Solid State Chem.* **12**, 362–369.
WELLS, A. F. (1962). *Structural Inorganic Chemistry*, 3rd ed., pp. 103–104. Oxford University Press.